Supplementary Material for
"Satellite Measurements Reveal Persistent Small-Scale Features in Ocean Winds"
by D. B. Chelton, M. G. Schlax, M. H. Freilich and Ralph F. Milliff

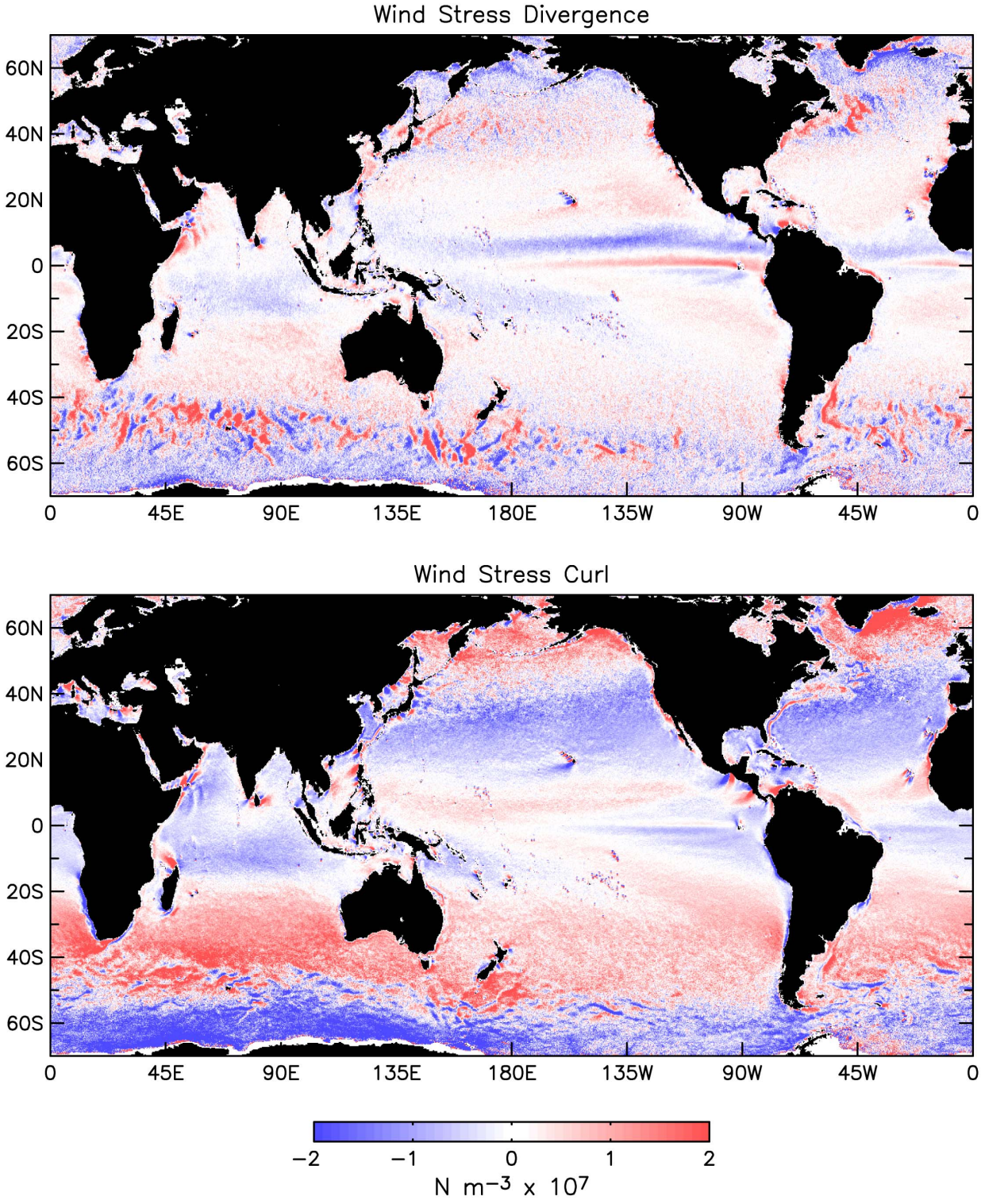

Fig. S1. Global 4-year average (August 1999–July 2003) divergence and curl of the wind stress field computed from QuikSCAT data as described in the text. This is an electronic version of Fig. 1 of the text. The small-scale features in any particular geographical region can be viewed using the magnifying tool in Adobe Acrobat Reader.

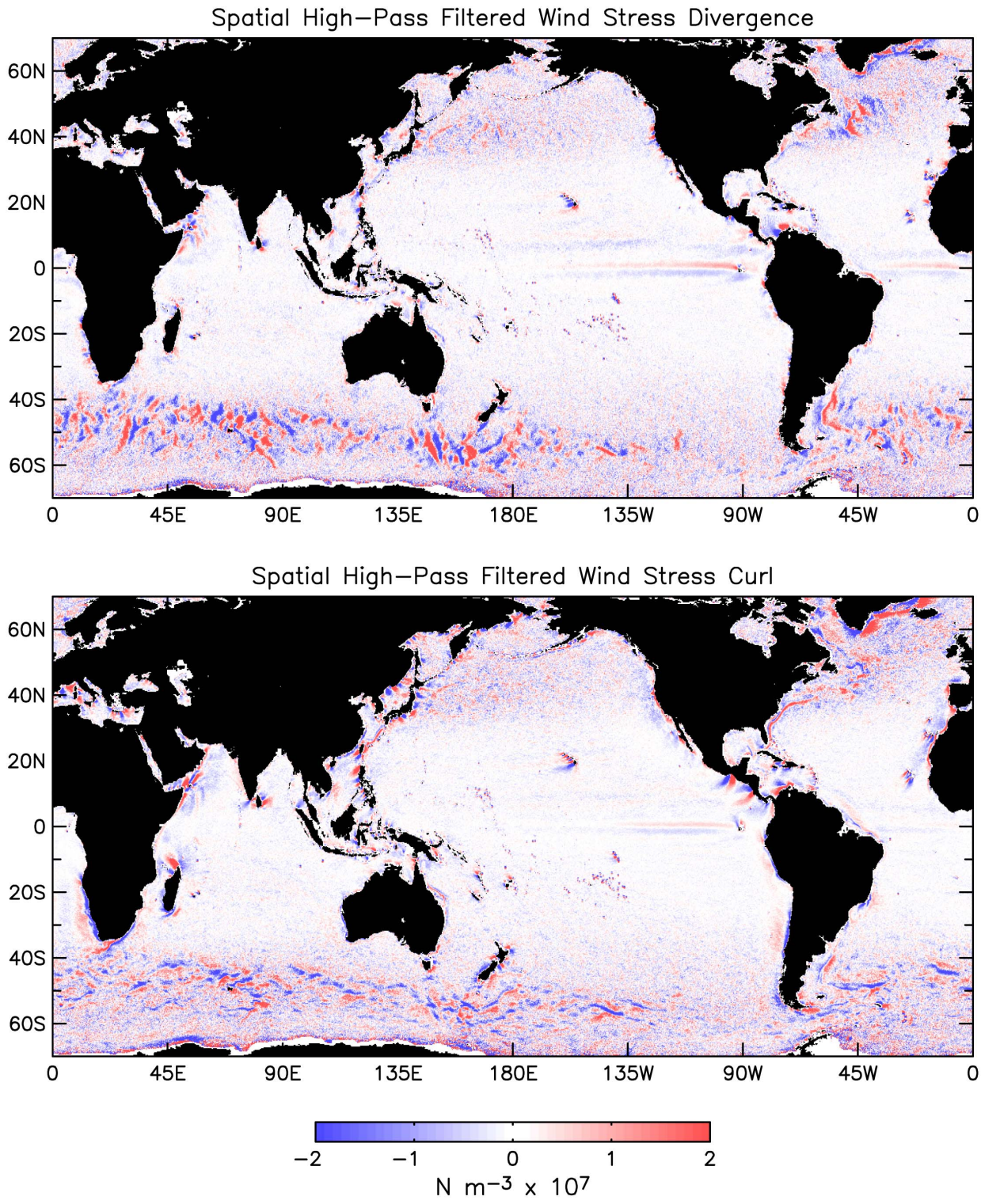

Fig. S2. Spatially high-pass filtered 4-year average (August 1999–July 2003) divergence and curl of the wind stress computed from QuikSCAT data. The filtering details are described in the text. This is an electronic version of the spatially high-pass filtered wind stress curl in Fig. 3 of the text, extended to include the spatially high-pass filtered divergence. The small-scale features in any particular geographical region can be viewed using the magnifying tool in Adobe Acrobat Reader.

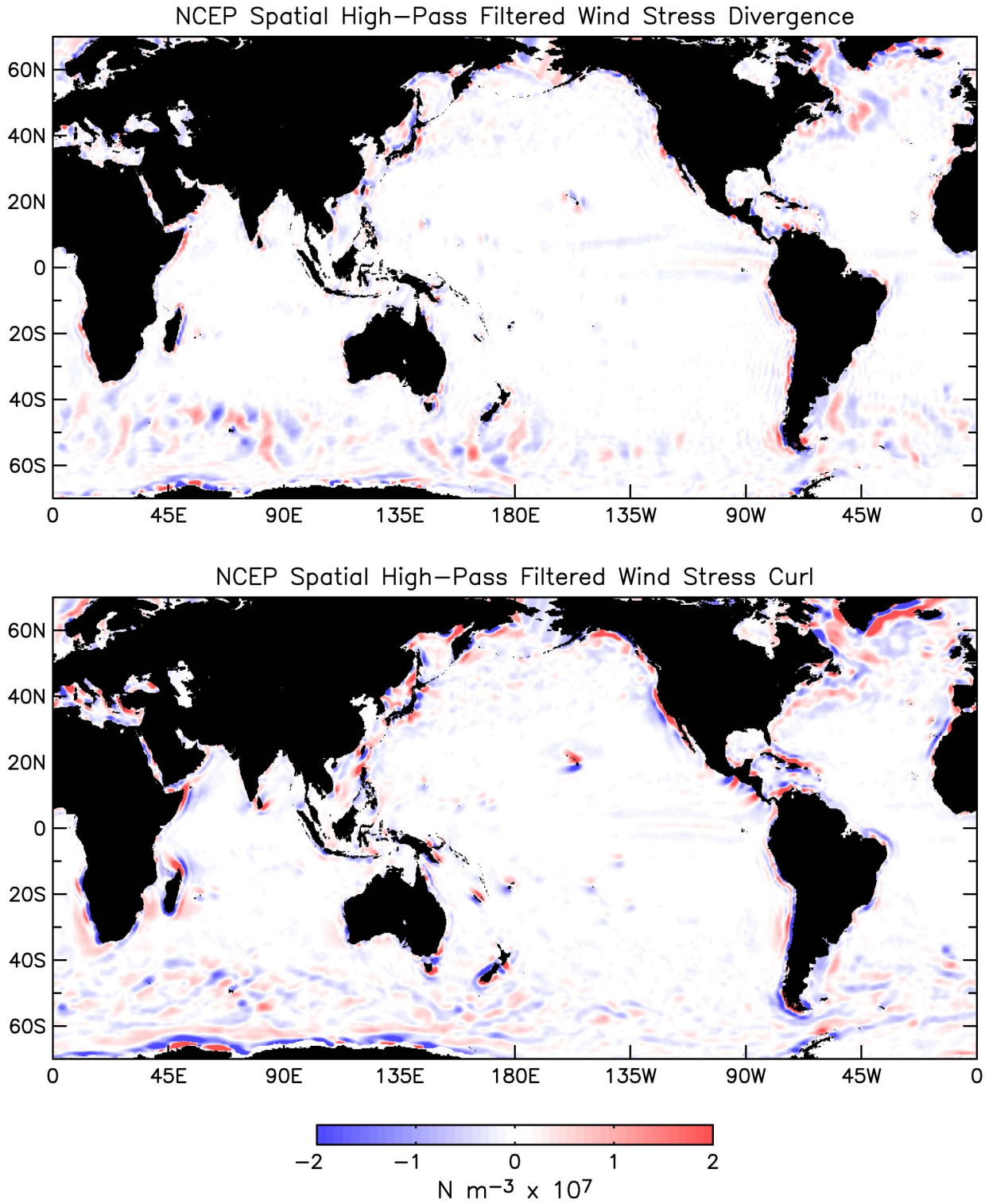

Fig. S3. The same as Fig. S2, except computed from the 1º by 1º by 6-hour analyses of winds at 10 m from the U.S. National Centers for Environmental Prediction (NCEP) operational numerical weather prediction model. Some of the small-scale features in the QuikSCAT divergence and curl fields are also evident in the NCEP fields, but generally with smaller amplitudes and larger scales. The alternating bands of positive and negative divergence and curl near many of the continental boundaries (especially evident off the west coasts) are artifacts of spectral truncation of mountain topography in the spherical harmonic NCEP model (*S1*).

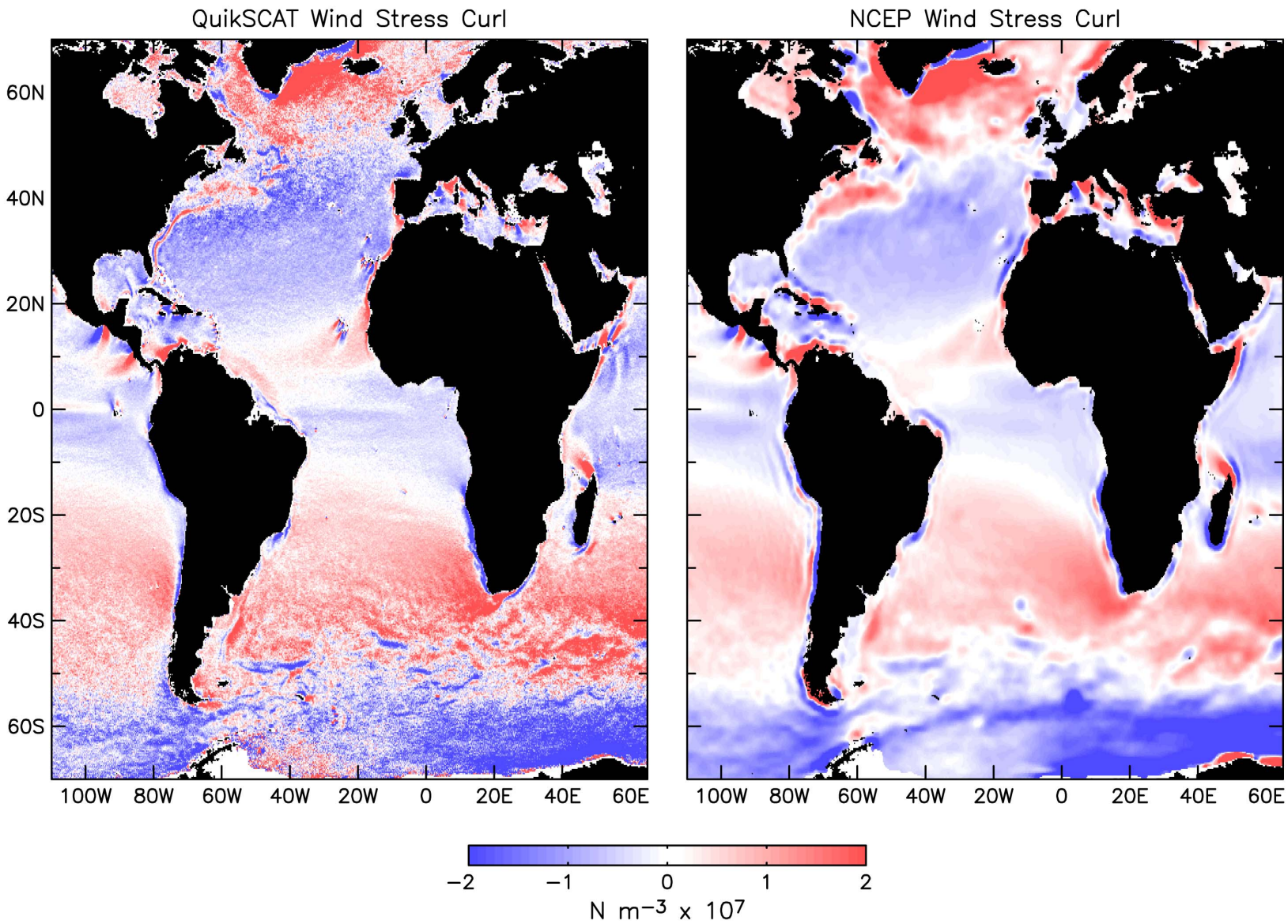

Fig. S4. Four-year averages (August 1999–July 2003) of the wind stress curl over the Atlantic, eastern Pacific and western Indian oceans computed from QuikSCAT measurements (left) and the NCEP model winds. This is the same as Fig. 2 of the text, except for an expanded geographical domain. The alternating bands of positive and negative curl in the right panel near many of the continental boundaries (especially evident off the west coast of South America) are artifacts of spectral truncation of mountain topography in the spherical harmonic NCEP model (*S1*). Similarly, the two isolated patches of negative curl in the NCEP field in the South Indian and South Atlantic oceans centered near Marion Island (38ºE, 47ºS) and Tristan de Cunha (12ºW, 37ºS) are likely artifacts of spectral truncation of island topography in the NCEP model.

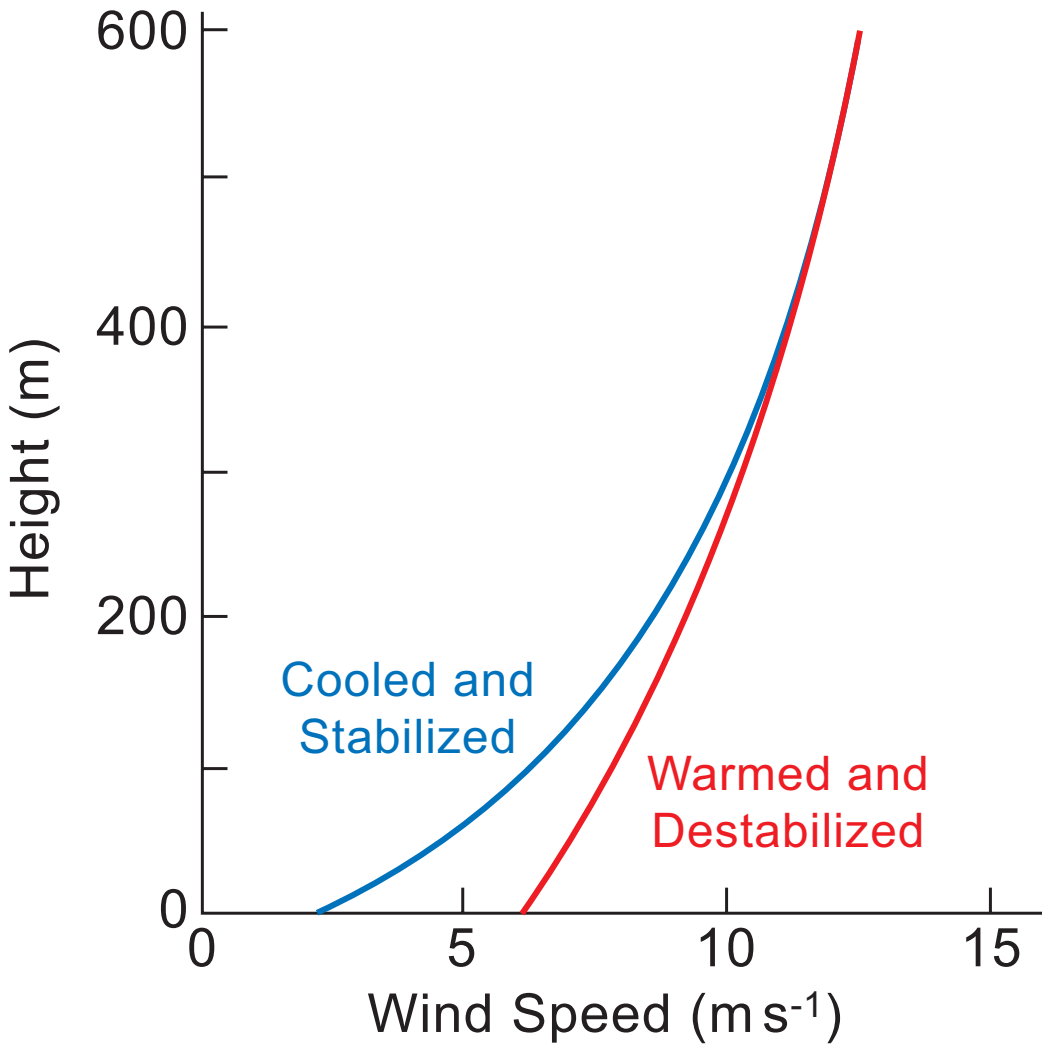

Fig. S5. Schematic illustration of wind variations in the marine atmospheric boundary layer (MABL) induced by small-scale features in the SST field (*S1-S5*). Cooling over cool water increases stratification and stabilizes the MABL. This inhibits vertical mixing by turbulence and convection, decoupling the surface winds from the winds aloft and increasing the wind shear near the sea surface (blue curve). Heating over warm water decreases stratification and destabilizes the MABL. This enhances vertical turbulent mixing, which deepens the MABL and mixes momentum downward from aloft, decreasing the wind shear near the sea surface (red curve). Deepening of the MABL over warm water has been observed directly (*S6, S7*) and inferred from satellite measurements of increased low-level cloudiness (*S8–S10*). Cooling and warming of the MABL also create an enhanced pressure gradient in the direction of the SST gradient (*S4, S5*). Small imbalances between the pressure gradient force and frictional effects from vertical turbulent mixing accelerate the flow in regions of strong downwind SST gradients, resulting in higher surface wind speeds over warm water and lower surface wind speeds over cool water.

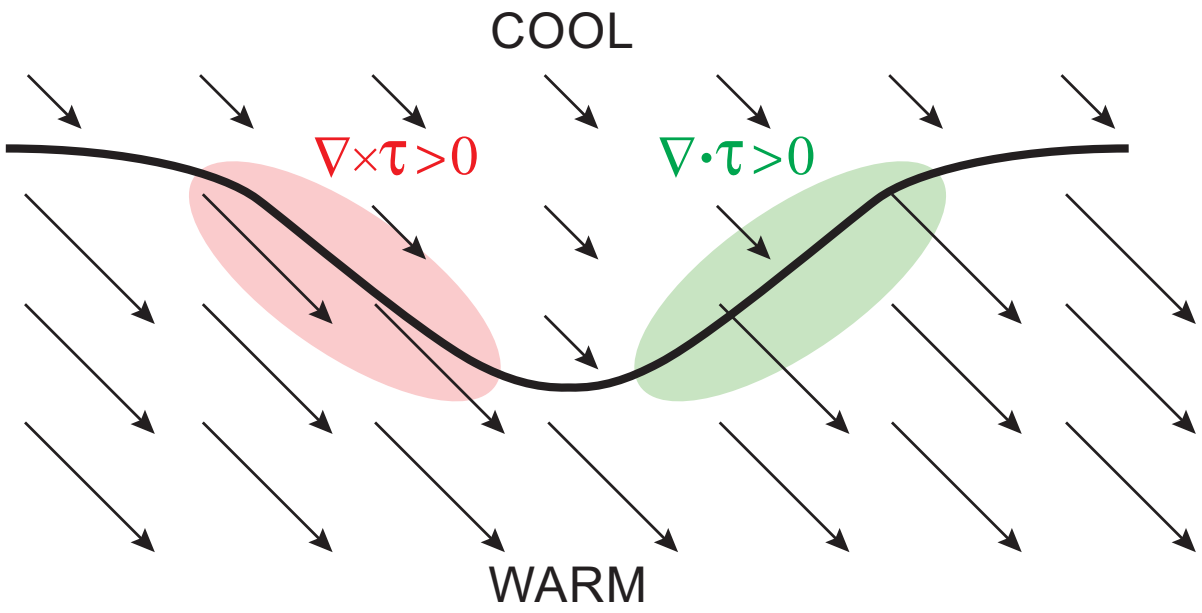

Fig. S6. Schematic illustration of the divergence and curl of the wind stress τ resulting from spatial variations of the SST effects on the surface winds summarized in Fig. S5. Near a meandering SST front (heavy black line), surface wind speeds are lower over cool water and higher over warm water, shown qualitatively by the lengths of the vectors. Acceleration where winds blow across isotherms generates divergence, $\nabla \cdot \tau$ (green area). Lateral variations where winds blow parallel to isotherms generate curl, $\nabla \times \tau$ (red area). The magnitudes of the divergence and curl perturbations are proportional to the magnitudes of the downwind and crosswind SST gradients, respectively (see Fig. 4 in the text).

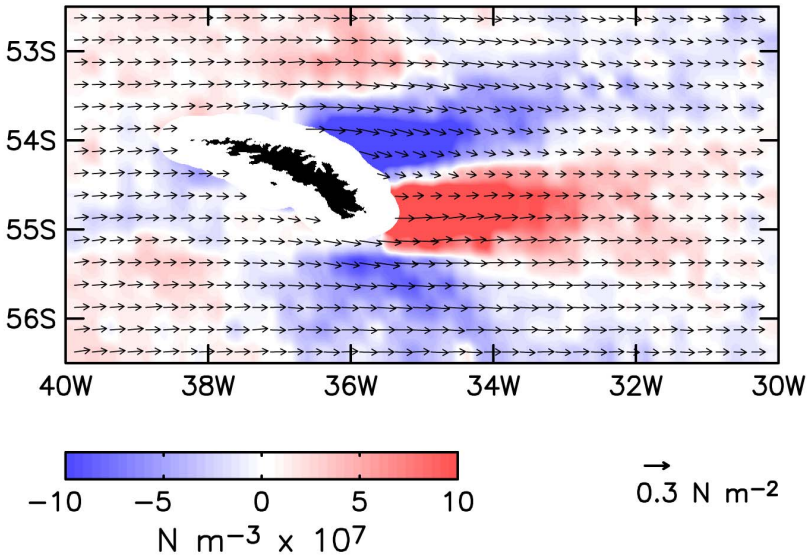

Fig. S7. The wind stress vectors and curl around South Georgia Island in the South Atlantic averaged over conditions during which the winds were within ±15° of the prevailing westerly wind direction in this region. This accounts for about 20% of the QuikSCAT overpasses. To accommodate the large dynamic range of the curl in the lee of the island, the color scale differs from the color scales in Figs. S1-S4 and in the curl figures in the text. Distortion of the wind field by 2934-m Mount Paget and twelve other mountain peaks exceeding 2000 m can be detected in the curl field more than 500 km downwind of the island. Wind shadows develop in the lee of South Georgia Island when the winds blow from other directions as well (*S12*).

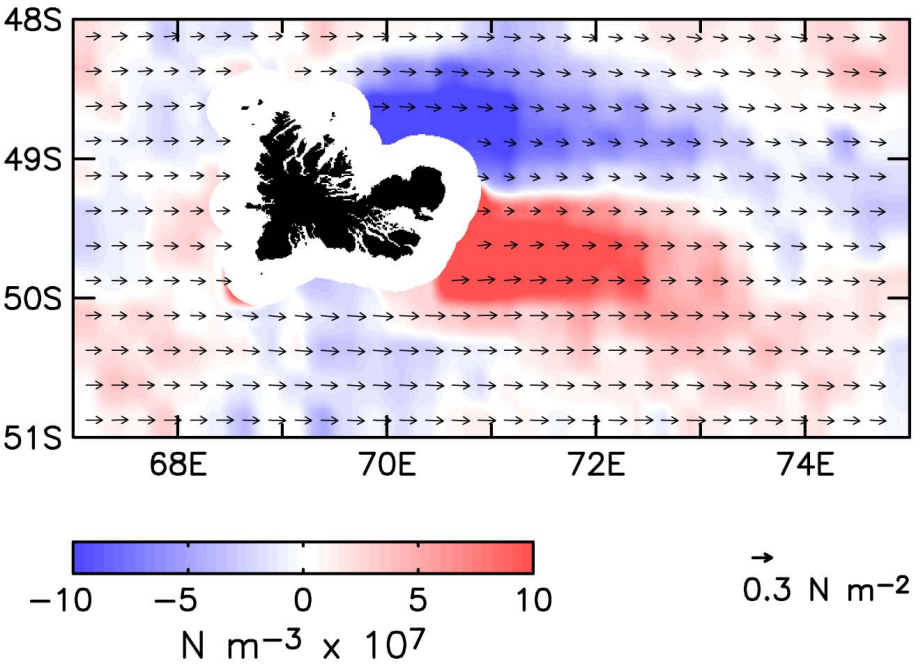

Fig. S8. The same as Fig. S7, except the prevailing wind stress vectors and curl around Kerguelen Island in the South Indian Ocean. Winds within ±15º of the prevailing westerly wind direction account for about 30% of the QuikSCAT overpasses. Distortion by 1850-m Mount Ross, the broad 1050-m plateau of Cook Glacier, and several smaller mountain peaks with elevations near 1000 m can be detected in the curl field more than 250 km downwind of the island.

References Cited in the Supporting Online Material

S1. R. F. Milliff, J. Morzel, *J. Atmos. Sci.* **58**, 108 (2001).
S2. W. R. Sweet, R. Fett, J. Kerling, P. LaViolette, *Mon. Wea. Rev.* **108**, 1042 (1981).
S3. J. M. Wallace, T. P. Mitchell, C. Deser, *J. Climate*. **15**, 1492 (1989).
S4. S. P. de Szoeke, C. S. Bretherton, in preparation.
S5. M. F. Cronin, S.-P. Xie, H. Hashizume, *J. Climate*. **16**, 3050 (2003).
S6. R. J. Small, S.-P. Xie, Y. Wang, *J. Climate*. **16**, 3724 (2003).
S7. M. R. Jury, *J. Geophys. Res.* **99,** 3297 (1994).
S8. H. Hashizume *et al.*, *J. Climate*. **15**, 3379 (2002).
S9. C. Deser, J. J. Bates, S. Wahl, *J. Climate*. **6**, 1172 (1993).
S10. H. Hashizume, S.-P. Xie, W. T. Liu, K. Takeuchi, *J. Geophys. Res.* **106**, 10,173 (2001).
S11. S.-P. Xie, W. T. Liu, Q. Liu, M. Nonaka, *Science*. **292**, 2057 (2001).
S12. M. H. Freilich, B. Vanhoff, D. G. Long, R. S. Dunbar, in preparation.